IJMMM International Journal of Minerals, Metallurgy and Materials 矿物冶金与材料学报（英文版）

Scale-up validation of an integrated process for boron/iron separation and boric acid preparation from ludwigite ore

Jinxiang You, Xin Zhang, Mingjun Rao, Jun Luo, Zhiwei Peng, and Guanghui Li

Cite this article as:
Jinxiang You, Xin Zhang, Mingjun Rao, Jun Luo, Zhiwei Peng, and Guanghui Li, Scale-up validation of an integrated process for boron/iron separation and boric acid preparation from ludwigite ore, *Int. J. Miner. Metall. Mater.*, 33(2026), No. 4, pp. 1104-1115. https://doi.org/10.1007/s12613-025-3238-z

---

Articles you may be interested in

Jinxiang You, Jing Wang, Mingjun Rao, Xin Zhang, Jun Luo, Zhiwei Peng, and Guanghui Li, An integrated and efficient process for borax preparation and magnetite recovery from soda-ash roasted ludwigite ore under CO–CO_2–N_2 atmosphere, *Int. J. Miner. Metall. Mater.*, 30(2023), No. 11, pp. 2169-2181. https://doi.org/10.1007/s12613-023-2643-4

Qipeng Bao, Lei Guo, Hong Yong Sohn, Haibin Zuo, Feng Liu, Yongliang Gao, and Zhancheng Guo, New process for treating boron-bearing iron ore by flash reduction coupled with magnetic separation, *Int. J. Miner. Metall. Mater.*, 31(2024), No. 3, pp. 473-484. https://doi.org/10.1007/s12613-023-2756-9

Haoyan Sun, Zheng Zou, Meiju Zhang, and Dong Yan, Fluidized magnetization roasting of refractory siderite-containing iron ore via preoxidation–low-temperature reduction, *Int. J. Miner. Metall. Mater.*, 30(2023), No. 6, pp. 1057-1066. https://doi.org/10.1007/s12613-022-2576-3

Jing Chen, Yuqi Zhong, Boqi Wang, Jun Luo, Zhiwei Peng, Yanhu Chen, Guanghui Li, and Mingjun Rao, Na_2SO_4-assisted reductive roasting for enhanced Ni and Co recovery from limonitic laterite: Mechanism and pilot-scale rotary kiln validation, *Int. J. Miner. Metall. Mater.*, 32(2025), No. 10, pp. 2418-2428. https://doi.org/10.1007/s12613-025-3116-8

Zhenxing Liu, Fangjie Deng, Yuan Zhou, Yanjie Liang, Cong Peng, Bing Peng, Feiping Zhao, Zhihui Yang, and Liyuan Chai, Effect of transport agent boron triiodide on the synthesis and crystal quality of boron arsenide, *Int. J. Miner. Metall. Mater.*, 29(2022), No. 4, pp. 662-670. https://doi.org/10.1007/s12613-022-2438-z

Aoyu Zhang, Lida Song, Zhaoyang Dong, Runguo Zheng, Zhishuang Song, Yanguo Liu, Jingsheng Xu, and Zhiyuan Wang, B-coating modulation strategy serving ultrahigh nickel cathodes, *Int. J. Miner. Metall. Mater.*, 32(2025), No. 8, pp. 2007-2014. https://doi.org/10.1007/s12613-025-3093-y

IJMMM WeChat

QQ author group

INTERNATIONAL JOURNAL OF
Minerals, Metallurgy and Materials

Volume 33, Number 4, April 2026
Page 1104

Research Article https://doi.org/10.1007/s12613-025-3238-z

Scale-up validation of an integrated process for boron/iron separation and boric acid preparation from ludwigite ore

Jinxiang You[1,2], *Xin Zhang*[3], *Mingjun Rao*[3)✉], *Jun Luo*[4], *Zhiwei Peng*[3], *and Guanghui Li*[3)✉]

1) State key Laboratory of Coking Coal Resources Green Exploitation, China University of Mining and Technology, Xuzhou 221116, China
2) Chinese National Engineering Research Center of Coal Preparation and Purification, China University of Mining and Technology, Xuzhou 221116, China
3) School of Minerals Processing and Bioengineering, Central South University, Changsha 410083, China
4) College of Chemistry and Chemical Engineering, Central South University, Changsha 410083, China
(Received: 8 April 2025; revised: 23 July 2025; accepted: 24 July 2025)

Abstract: Ludwigite ore is a strategic mineral resource unique to China. Its efficient and comprehensive utilization is of paramount importance for ensuring the healthy and sustainable development of China's industry and national defense security. This study presents and validates a scale-up integrated process for separating boron and iron from boron–iron mixed concentrate (BIMC) and producing reduced iron powder and high-purity boric acid. The process involves reductive soda-ash roasting in a rotary kiln, followed by wet-grinding, magnetic separation, and fractional crystallization. Under optimized parameters, the process achieved a boron leaching efficiency of 70.23%, an iron grade in the magnetic concentrate of 94.12wt%, and a corresponding recovery of 93.35%. The recovered reduced iron powder can be used as feed for short-process steelmaking. The boron-rich liquor was then used to prepare high-purity boric acid (>99wt%) with a regular morphology by adjusting the pH with sulfuric acid, and the corresponding aqueous chemical behaviors were investigated. This integrated process offers a promising approach for the efficient and environmentally friendly utilization of boron–iron complex ore.

Keywords: ludwigite ore; reductive-soda roasting; reduced iron powder; scale-up validation; solution chemistry; boric acid

1. Introduction

The Liaoning Fengcheng Wengquangou boron–iron mine (named as ludwigite ore), with a known reserve of 283 million tons, accounts for 58% of China's total known solid boron reserve. This mine contains a variety of minerals, including boron, magnesium, and iron, primarily in the form of szaibelyite, serpentine, and magnetite. The efficient and comprehensive utilization of the ludwigite ore has been a key focus due to its abundant boron and iron reserves, despite its low grade and complex mineral composition [1–4].

Current physical separation methods for beneficiating ludwigite ore yield both boron concentrate and boron-containing iron concentrate, which are used for borax production and ironmaking, respectively. The CO_2-soda method employed to produce borax from boron concentrate generates a significant amount of alkali-containing waste (boron mud), which is currently non-recyclable and classified as hazardous waste, posing a significant environmental concern [5–8]. Furthermore, the sintering–blast furnace method used for ironmaking of the boron-containing iron concentrate results in low value-added utilization of the boron component [9–10].

To address these challenges, a multi-step process involving reductive soda-ash roasting, grind–leaching and magnetic separation was previously proposed [11–12]. This method demonstrated improved recoveries of boron and iron, enabling the comprehensive utilization of valuable components. Approximately 70wt% of the boron was extracted into the liquor, and 95wt% of the metallic iron powder was recycled by magnetic separation. The non-magnetic tailings were further leached at 453 K to recycle the residual boron and sodium, and the leached residue (magnesia-rich residue) can be used to prepare magnesia-based refractory materials, realizing the comprehensive utilization of valuable components [13].

Although the proposed process has demonstrated significant advantages in laboratory-scale studies, such as a streamlined process flow, low energy consumption, and high recoveries of boron and iron, its feasibility for industrial application still necessitates validation through systematic scale-up experiments. Laboratory-scale reductive roasting experiments, particularly conducted using a muffle furnace, exhibit notable limitations. Firstly, the static heating methods employed struggle to replicate the dynamic thermal field environments encountered in actual production. Secondly, small-scale setups fail to accurately reflect the mass and heat transfer characteristics observed at an industrial scale. Through scale-up experimental studies, critical issues that are often overlooked in small-scale research can be effectively identified and addressed. Hence, conducting scale-up experiments in a rotary kiln not only verifies the feasibility of industrial application of the reductive soda-ash roasting process, but

✉ Corresponding authors: Mingjun Rao E-mail: mj.rao@csu.edu.cn; Guanghui Li E-mail: liguangh@csu.edu.cn

also provides critical process parameters and a scientific basis for industrial scale design. This research offers significant engineering guidance for the efficient and clean utilization of ludwigite resources.

This study further investigates the application of this process at a scale-up rotary kiln, demonstrating enhanced recoveries of boron and iron, as well as the preparation of high-purity boric acid from the boron-rich liquor. These results highlight the potential for industrial-scale utilization of Wengquangou boron–iron complex ore.

2. Experimental

2.1. Materials

The boron–iron mixed concentrate (BIMC) is an intermediate product obtained through the combined magnetic and gravity separation of ludwigite ore from Liaoning Shougang Iron Boron Co., Ltd., China. The chemical composition of the BIMC sample contains 46.89wt% of total iron (TFe), 5.80wt% B_2O_3, 15.31wt% MgO, and 7.64wt% SiO_2, as shown in Table S1. X-ray diffraction (XRD) pattern of the BIMC shows that the main phase composition was magnetite, szaibelyite, and lizardite (Fig. S1).

Lignite was used as a reducing agent, and the proximate analysis and ash composition of lignite are listed in Table S2. The contents of fixed carbon (FC_{ad}), volatile matter (V_{ad}), ash (A_{ad}), and moisture (M_{ad}) are 60.32wt%, 19.84wt%, 10.33wt%, and 9.51wt%, respectively. The anhydrous sodium carbonate and sulfuric acid are of industrial grade purity, while the sodium bicarbonate and boric acid used are of analytical grade.

2.2. Methods

2.2.1. Reductive soda-ash roasting

Reductive soda-ash roasting experiments were conducted using a rotary kiln with a diameter of 1.0 m and a length of 0.55 m. The mixture of BIMC, soda-ash, and lignite were mixed and briquetted using a briquetting machine. Preliminary experiments in laboratory scale have determined that the suitable roasting parameters: soda-ash dosage of 25wt%, roasting temperature of 1323 K. Therefore, a soda-ash dosage of 25wt% was chosen for the rotary kiln experiments. The rotary kiln was preheated to 1273 K, and then 30 kg of dry briquettes were introduced. Additionally, 10 kg lump coal (5–20 mm) was also added to the rotary kiln to maintain the reductive atmosphere. The kiln was heated for 45–60 min and maintained at 1323 K for 60 min. After reduction, the roasted briquettes were discharged from the kiln and covered with fine coal to prevent reoxidation.

2.2.2. Grind–leaching and magnetic separation

After reduction, the roasted briquettes were crushed to a particle size of less than 1 mm and then subjected to wet grinding with a pulp concentration of 50wt% for 20 min. The fineness of the grinding product of −45 μm was 85wt%. The pulp was filtered to obtain leached liquor (boron-rich liquor) and leached residue. The boron-rich liquor was used to synthesize boric acid, while the leached residue was subjected to magnetic separation to produce reduced iron powder.

Magnetic separation was conducted using a magnetic drum separator (XCRS74-Φ400 × 300) with a magnetic field intensity of 79.6 kA·m^{-1}. The obtained magnetic concentrate and tailing were dried in a vacuum oven at 373 K for 6 h. The boron leaching efficiency (χ), iron grade in the magnetic concentrate (ω_1), and iron recovery (η) were used to evaluate the process. These parameters were calculated as follows:

$$\chi = \frac{c \times V}{m_0 \times \alpha} \times 100\% \quad (1)$$

$$\eta = \frac{m_1 \times \omega_1}{m_0 \times \omega_0} \times 100\% \quad (2)$$

where c and V are the concentration (g/L) and volume (L) of leached liquor, respectively; m_0 and α represent the mass (g) and boron content (wt%) of the feed, respectively; m_1 is the mass of magnetic concentrate (g); ω_1 and ω_0 represent the iron grade in the magnetic concentrate (wt%) and feed (wt%), respectively.

2.2.3. Preparation of boric acid

The preparation of boric acid was conducted in a 5 L three-necked flask equipped with a pH meter, heated by a thermostatic water bath, and agitated by a stirrer. 50vol% H_2SO_4 was introduced into the liquor using a peristaltic pump, and the reaction temperature was maintained at 333 K. After reaction, the liquor was then subjected to fractional crystallization to obtain boric acid at 308 K and sodium sulfate at 283 K. The crystallization ratio of boric acid was calculated as follows:

$$\psi = \left(1 - \frac{c_2 \times V_2}{c_1 \times V_1}\right) \times 100\% \quad (3)$$

where ψ (%) represents the crystallization ratio percentage of boric acid; c_1 and V_1 are the concentration (g/L) and volume (L) of boron-rich liquor before crystallization, respectively; c_2 and V_2 are the concentration (g/L) and volume (L) of boron-containing liquor after crystallization, respectively. The schematic flow of preparation of reduced iron powder and synthesis of boric acid is illustrated in Fig. 1.

2.3. Analytical methods

The metallic iron and TFe contents in the samples were determined by the chemical titration method. The boron content in both solid and liquor samples was analyzed using an inductively coupled plasma optical emission spectrometer (ICP-OES, Optima, 5300 DV, USA). The contents of other elements were determined by atomic absorption spectroscopy. XRD (Rigaku, ultima IV, Japan) was analyzed using a Cu K_α X-ray source. Microstructures were observed using a scanning electron microscope (SEM, TESCAN, MIRA4, Czech) and electron probe micro analyzer (EPMA, EPMA-1720 Shimadzu, Japan). Thermodynamic analysis was conducted using the FactSage 8.0 software. Raman spectra were performed using a HORIBA Scientific LabRAM HR Evolution device with a laser excitation wavelength of 514 nm at room temperature. Nuclear magnetic resonance (NMR) measurement (BRUKER Avance NEO 600, Germany) was employed to analyze the variation of boron and carbon species in the liquor.

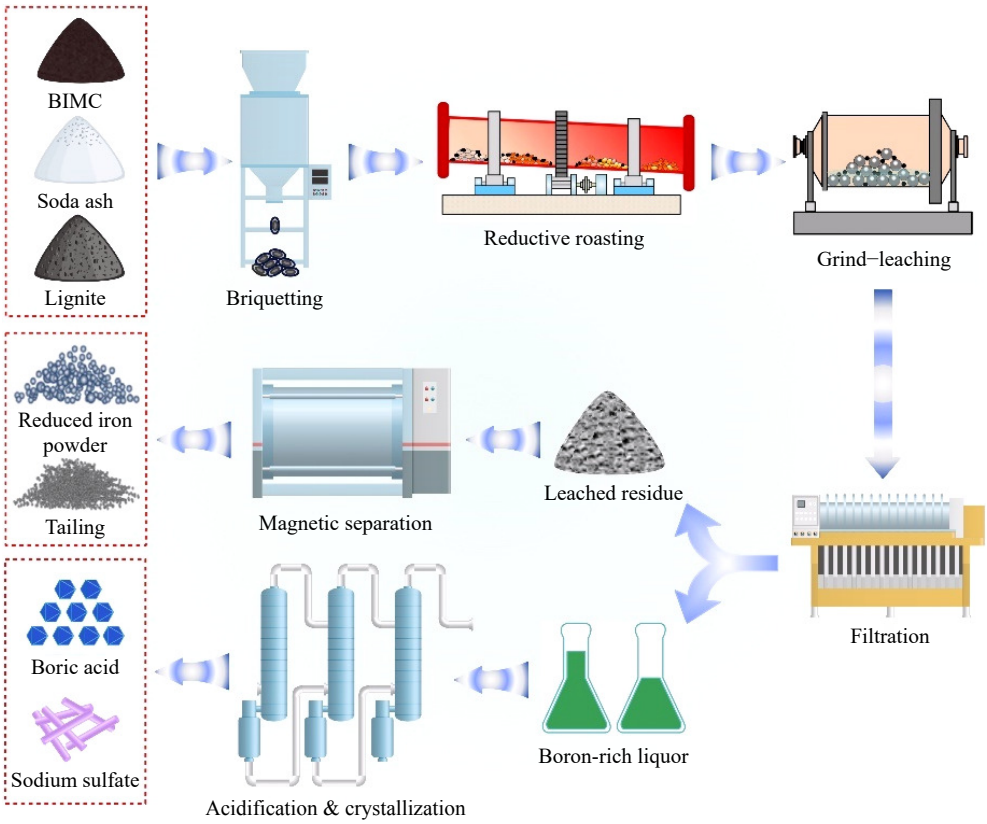

Fig. 1. Schematic diagram of preparation of reduced iron powder and boric acid.

3. Results and discussion

3.1. Preparation of reduced iron powder

3.1.1. Reductive soda-ash behavior

Previous preliminary experiments have proven that a soda-ash dosage of 25wt%, a reductive temperature of 1323 K, and a reductive duration of 60 min were suitable reduction roasting conditions [11,13]. Thus, the dry briquettes were roasted at 1323 K for 60 min, with varying dosages of lignite as the reductant. As shown in Fig. 2(a), the iron metallization ratio of roasted ore increased with the addition of lignite. The iron metallization ratio rose rapidly from 33.68wt% to 91.23wt% as the lignite dosage increased from 0 to 8wt%, and then only slightly to 93.59wt% when the dosage was further increased to 10wt%. Fig. 2(b) shows the XRD patterns of roasted ores with varying additions of lignite, and the phase composition of roasted ores consisted of iron (Fe), magnesiowüstite ($Mg_xFe_{1-x}O$), and sodium magnesium silicate (Na_2MgSiO_4). During reduction, magnetite was reduced into wüstite and metallic iron (Eqs. (4)–(5)), while sodium carbonate reacted with boron-containing minerals and silicate minerals to generate water-soluble sodium borate ($NaBO_2$) and insoluble sodium magnesium silicate (Eqs. (6)–(7)). In addition, part of FeO would react with the produced MgO to form $Mg_xFe_{1-x}O$ by solid–solid reaction (Eq. (8)).

$$Fe_3O_4 + C = 3FeO + CO(g) \quad (4)$$

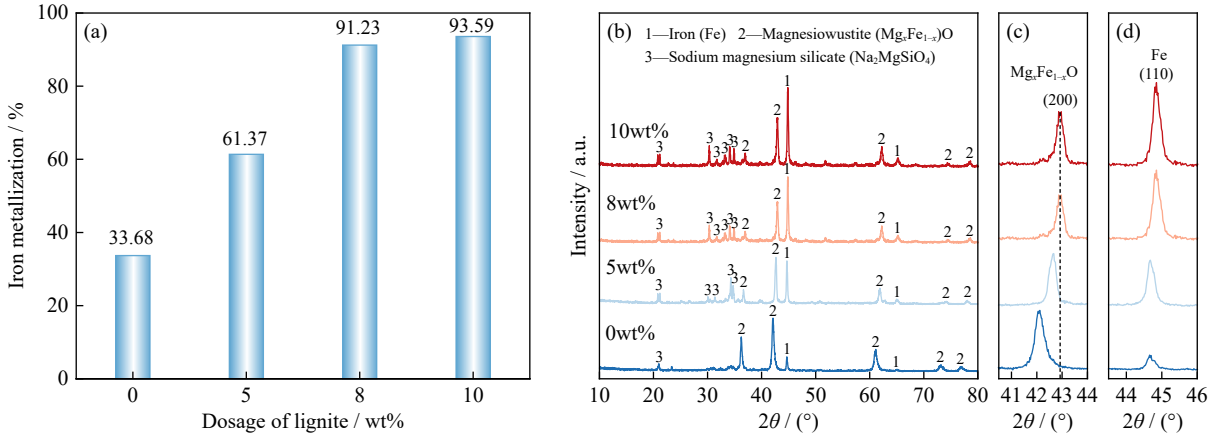

Fig. 2. (a) Effect of lignite dosage on the iron metallization ratio; (b) XRD patterns of roasted ores with different dosages of lignite, zoom-in portion of the XRD pattern for (c) the (200) crystal plane of $Mg_xFe_{1-x}O$ and (d) the (110) crystal plane of Fe.

$$FeO + CO = Fe + CO_2(g) \quad (5)$$

$$2MgBO_2(OH) + Na_2CO_3 = 2NaBO_2 + 2MgO + CO_2(g) + H_2O(g) \quad (6)$$

$$Mg_3Si_2(OH)_4O_5 + 2Na_2CO_3 = 2Na_2MgSiO_4 + MgO + 2CO_2(g) + 2H_2O(g) \quad (7)$$

$$xMgO + (1-x)FeO = Mg_xFe_{1-x}O \quad (8)$$

Notably, it was observed that the diffraction peak corresponding to the (200) crystal plane of $Mg_xFe_{1-x}O$ obviously shifted to the right side of 2θ, with increasing lignite addition (Fig. 2(c)), demonstrating that the interplanar space increased. This variation was attributed to the reduction of iron ions in the $Mg_xFe_{1-x}O$ phase to metallic iron, which subsequently migrated out of the crystal lattice. $Mg_xFe_{1-x}O$ phase gradually converted to periclase (MgO), accompanied by the reduction of iron ions in $Mg_xFe_{1-x}O$. Furthermore, the enhanced intensity of the diffraction peak corresponding to (110) crystal plane of metallic iron further confirmed this conclusion (Fig. 2(d)).

Scanning electron microscope-energy dispersive spectrometer (SEM-EDS) analysis of the roasted samples with different lignite additions were performed to reveal the microstructural evolution and phase composition, with the results illustrated in Fig. 3. According to Fig. 2(a), the iron metallization ratio was moderately unsatisfactory when the lignite ad-

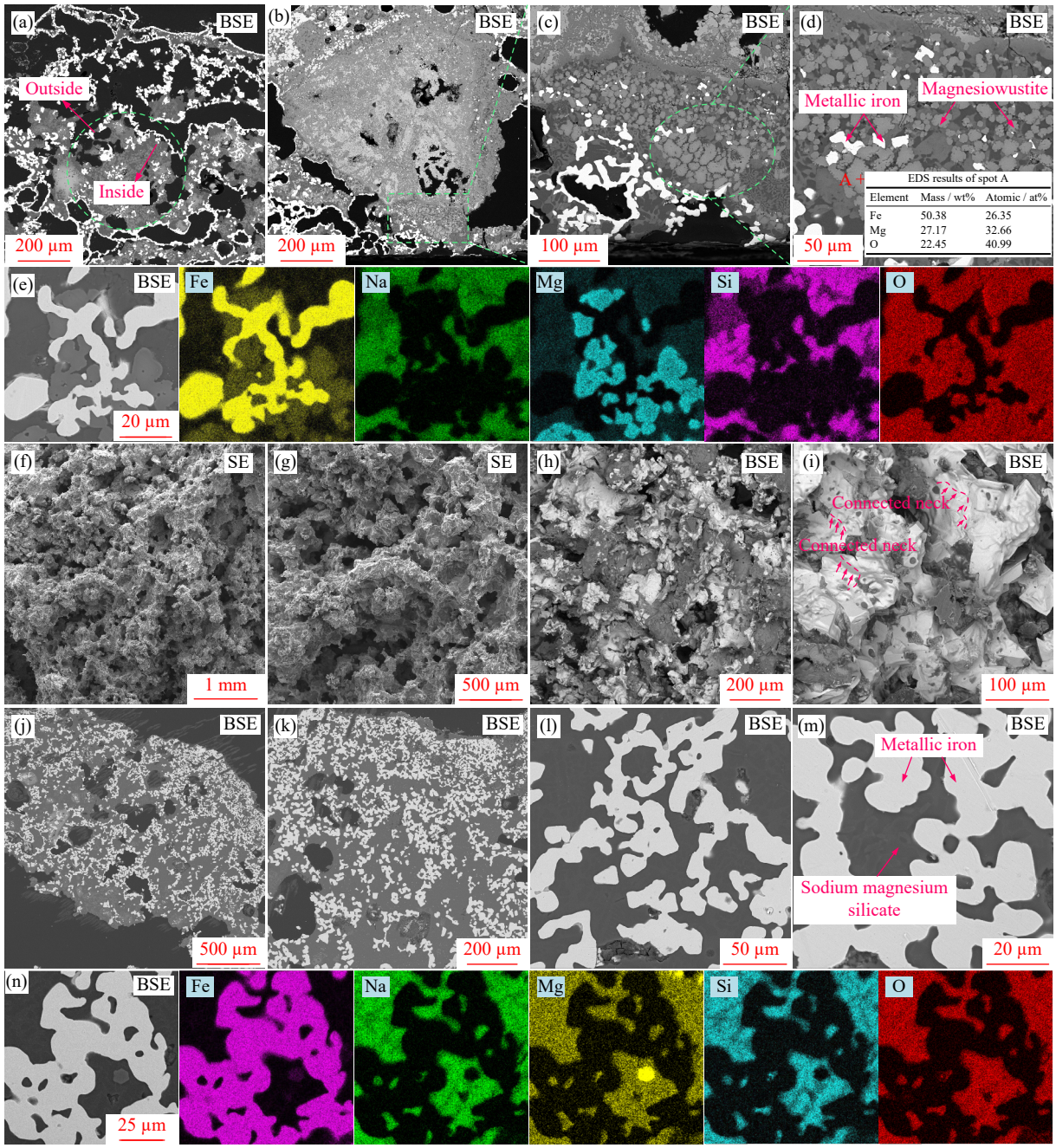

Fig. 3. SEM-EDS analysis of the roasted samples with (a–e) 5wt% and (f–n) 8wt% lignite addition (reductive temperature of 1323 K, duration time of 60 min). (BSE: backscattered electron; SE: secondary electron).

dition was 5wt%. It was evident that the roasted ore with 5wt% lignite presented a porous microstructure, with metallic iron grains aggregating in the outer region while the interior contained abundant relatively densely structured magnesiowüstite phase (Fig. 3(a)–(c)). EDS analysis results show that the iron content in the magnesiowüstite phase was relatively high (Fig. 3(d)). Additionally, Elemental mapping analysis also further confirmed the formation of magnesiowüstite (Fig. 3(e)). This indicated that the iron in the magnesiowüstite phase was not effectively reduced, leading to the lower iron metallization ratio.

When the lignite dosage increased to 8wt%, SEM images of the roasted sample show that the interior had a typical sponge iron structure, consisting of well-grown metallic iron grains with sizes of up to hundreds micrometer separated by pores (Fig. 3(f)–(h)). Moreover, it was observed that the metallic iron grains were interconnected through the connected neck, resulting in an increase in the size of iron particles. (Fig. 3(i)). SEM images and elemental mapping further indicated that the reduced sample was composed of metallic iron and sodium magnesium silicate, as confirmed by elemental mapping, and magnesiowüstite phase was not observed (Fig. 3(j)–(n)).

In order to reveal the boron activation during reduction, an EPMA analysis was further conducted to investigate the boron-containing phase. The microstructure revealed the presence of a sodium borate (spot 2) liquid phase, alongside metallic iron (spot 1) and sodium magnesium silicate (spot 3) (Fig. 4 and Table 1). It was assumed that the low-viscosity sodium borate liquid promoted the migration and growth of metallic iron grains during reduction. Upon cooling, the sodium borate transitioned into a homogeneous glass phase, while sodium magnesium silicate precipitated out.

3.1.2. Separation of boron and iron

After reduction, the roasted sample was subjected to grind–leaching and magnetic separation to separate boron and iron, respectively. Boron was dissolved into the pulp during wet grinding, owing to its soluble property.

$$NaBO_2 + 2H_2O(l) = Na^+(aq) + B(OH)_4^-(aq) \quad (9)$$

As shown in Fig. 5, the boron leaching efficiency was around 70% and was not significantly affected by the dosage of lignite. During reduction roasting, szaibelyite initially decomposed and formed suanite ($Mg_2B_2O_5$), which subsequently reacted with Na_2CO_3 to yield sodium borate and

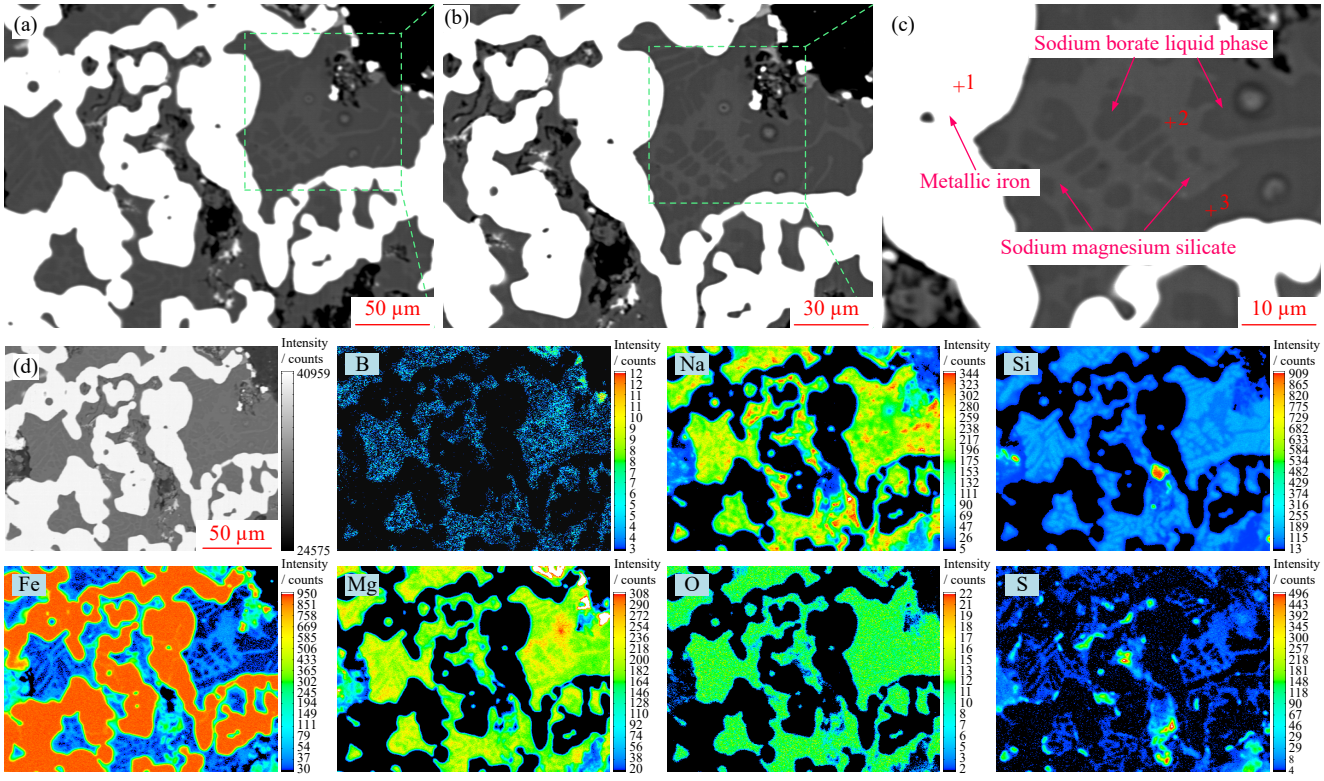

Fig. 4. (a–c) Microstructure and elemental (d) mapping analysis of the roasted sample (roasting temperature of 1323 K, duration time of 60 min, lignite dosage of 8wt%).

Table 1. Elemental mass distribution of the corresponding mineral phase in Fig. 4(c).

Spot	Element mass distribution / wt%					
	B	Fe	Mg	Si	Na	O
1	0.00	100.00	0.00	0.00	0.00	0.00
2	12.48	3.86	8.35	12.60	30.92	27.43
3	1.31	10.91	12.01	21.96	22.79	30.80

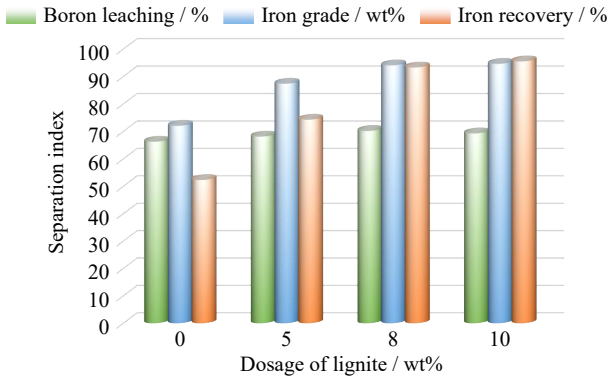

Fig. 5. Effect of dosage of lignite on the separation indices.

MgO. Hence, boron leaching efficiency was primarily affected by the dosage of Na_2CO_3. However, the iron grade in the magnetic concentrate and the iron recovery increased substantially as the lignite dosage rose from 0 to 8wt%, reaching 94.12wt% and 93.35%, respectively. Further increasing the lignite to 10wt% only led to a slight additional improvement. Therefore, a lignite dosage of 8wt% was deemed suitable.

Boron leaching was achieved during wet grinding, with approximately 70wt% of the boron being leached at a liquid-to-solid ratio of 1 mL/g and a grinding time of 20 min at room temperature. This was attributed to the coupling effect between grinding and leaching. Under the mechanochemical forces, the mineral particles were finely dissociated, exposing the sodium borate crystals to water and enhancing their dissolution (Fig. 6). The grinding also caused lattice distortion of the sodium borate, further improving the leaching efficiency.

3.1.3. Characterization of the reduced iron powder

The chemical composition of the reduced iron powder is shown in Table S3. The iron grade was 94.12wt%, making it suitable as a raw material for short-process steelmaking. The XRD pattern (Fig. S2(a)) confirmed the high purity of the reduced iron, with no impurity peaks detected. SEM images (Fig. S2(b)–(c)) revealed a block-like morphology with particle sizes around 50 μm.

3.2. Preparation of acid boric from the boron-rich liquor

3.2.1. Boron and silicon speciation in the aqueous solution

After grind–leaching and magnetic separation, the acquired boron-rich liquor was used to prepare boric acid, and the chemical composition of the boron-rich liquor is shown in Table 2. The concentration of boron and sodium are 4.15 and 14.68 g/L, respectively, while the main purity is silicon derived from the dissolution of sodium silicate.

Boron species commonly exist as various complex borate ions in aqueous solution due to complex hydrolysis reaction and polymerization, and they are commonly affected by the total boron concentration and pH value of the solution [14–16]. As shown in Fig. 7, at a low total boron concentration of 0.01 M, only the H_3BO_3 and $B(OH)_4^-$ species were observed. The molar fraction of H_3BO_3 decreased, while that of $B(OH)_4^-$ ion increased, as the pH rose from 0 to 14. At higher total boron concentrations of 0.1 M and above, additional polyborate species, such as $B_3O_3(OH)_4^-$ and $B_4O_5(OH)_4^{2-}$ were observed in the pH range of 6–13. The H_3BO_3 and HBO_2 species were predominant in the low pH range, while $B(OH)_4^-$ was stable in the high pH range.

The major impurity in the boron-rich liquor was silicon. Fig. 8 shows the distribution of silicon species as a function of pH and total silicon concentration. At low concentrations (0.001 M), the stable species were $SiO_2{\cdot}H_2O$ and $Si(OH)_4$ precipitates in the pH range of 0–9, while water-soluble silicate ions, such as $SiO(OH)_3^-$ and $SiO_2(OH)_2^{2-}$, existed at higher pH values of 10–14. As the total silicon concentration increased, the stable pH range of the $SiO_2{\cdot}H_2O$ precipitate widened, and the $Si(OH)_4$ species disappeared.

3.2.2. Boric acid synthesis by sulfuric acid acidification

The sulfuric acid acidification process involves the transformation of the boron and carbon species in the aqueous solution. Raman and NMR spectroscopy were employed to characterize the chemical reactions. As depicted in Fig. 9(a), the pH value of the solution gradually decreased with increasing acidification time, and it rapidly declined from pH of 7.0 to 2.0. Meanwhile, the crystallization ratio of boric acid rapidly increased from 24.47% to 93.14% as the pH

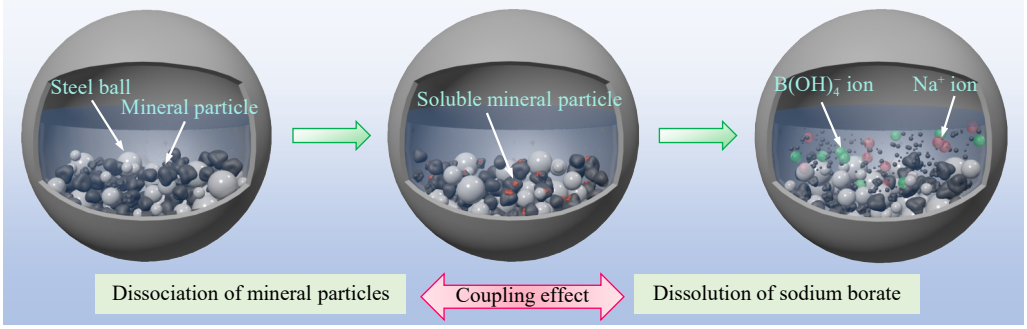

Fig. 6. Schematic diagram of the grind–leaching process.

Table 2. Chemical composition of the boron-rich liquor

B / (g·L^{-1})	Na / (g·L^{-1})	Si / (g·L^{-1})	Fe / (mg·L^{-1})	Mg / (mg·L^{-1})	Ca / (mg·L^{-1})	Al / (mg·L^{-1})
4.15	14.68	0.13	<1.0	<1.0	<1.0	<1.0

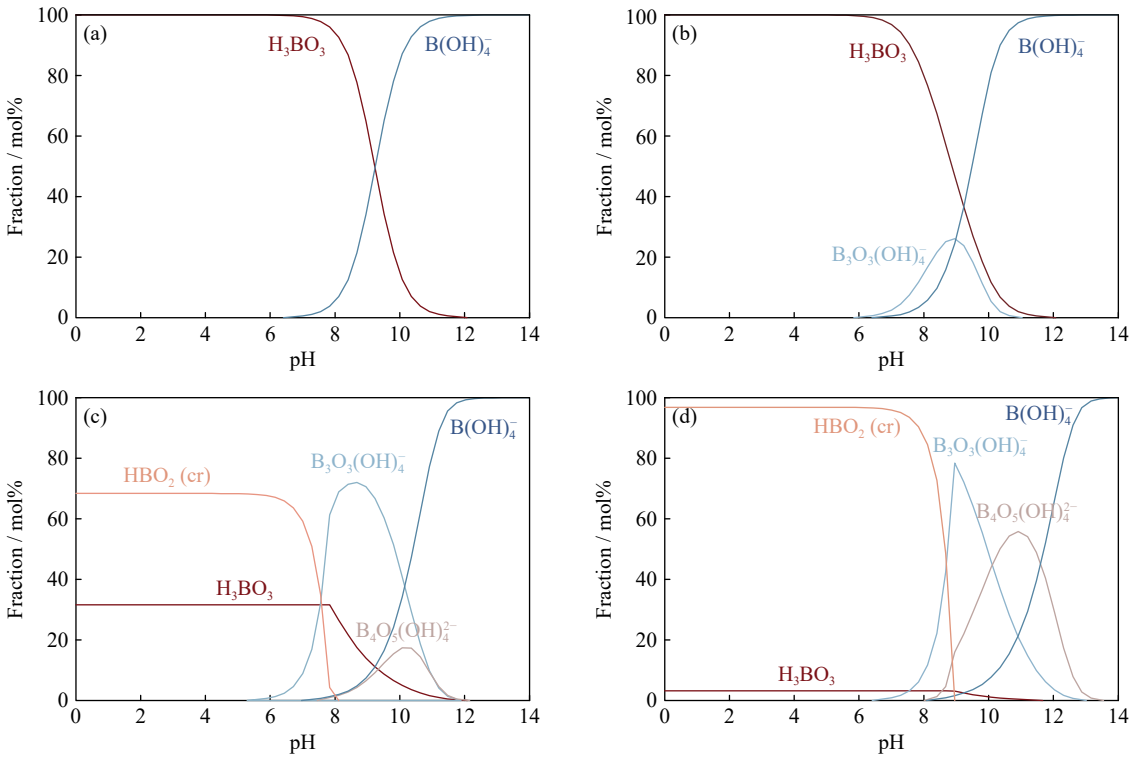

Fig. 7. Boron species distributed as a function of pH with different total boron concentration at 298 K: (a) 0.01 M, (b) 0.1 M, (c) 1.0 M, and (d) 10.0 M. (cr represents the crystal state).

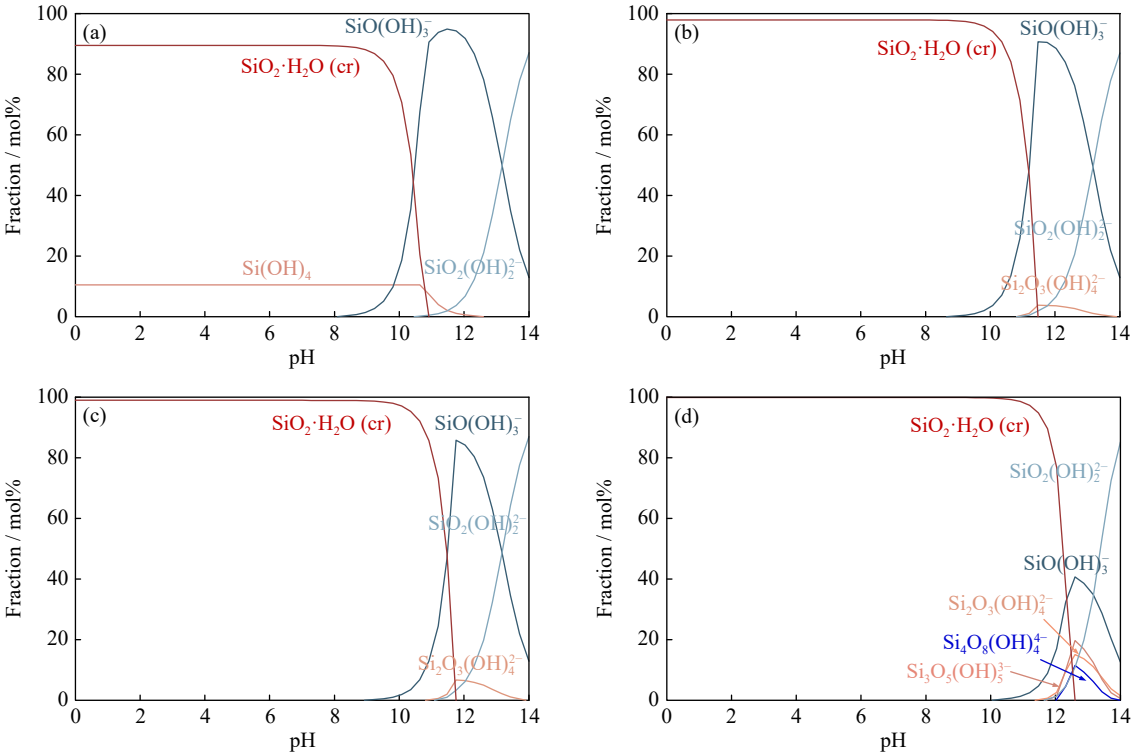

Fig. 8. Silica species distributed as a function of pH with different total silicon concentration at 298 K: (a) 0.001 M, (b) 0.005 M, (c) 0.01 M and (d) 0.1 M.

value decreased from 10.08 to 2.0, which was consistent with the boron aqueous chemistry results in Fig. 7.

Fig. 9(b) shows the Raman spectra varied with the pH values of the solution. The typical symmetric stretching vibrations of B–O bonds at 754 cm^{-1} indicated the presence of $B(OH)_4^-$ species in the aqueous solution, and the intensity of peak weakened and disappeared when the pH value decreased from 11.0 to 9.0 [17–18]. With the decrease of pH value, the intensity of emerging peaks at 458, 618, and 885 cm^{-1}, attributed to the vibrations of plane triangle B–O bonds in H_3BO_3 molecules, gradually enhanced, suggesting the presence of H_3BO_3 [19–21]. Meanwhile, the intensity of peak

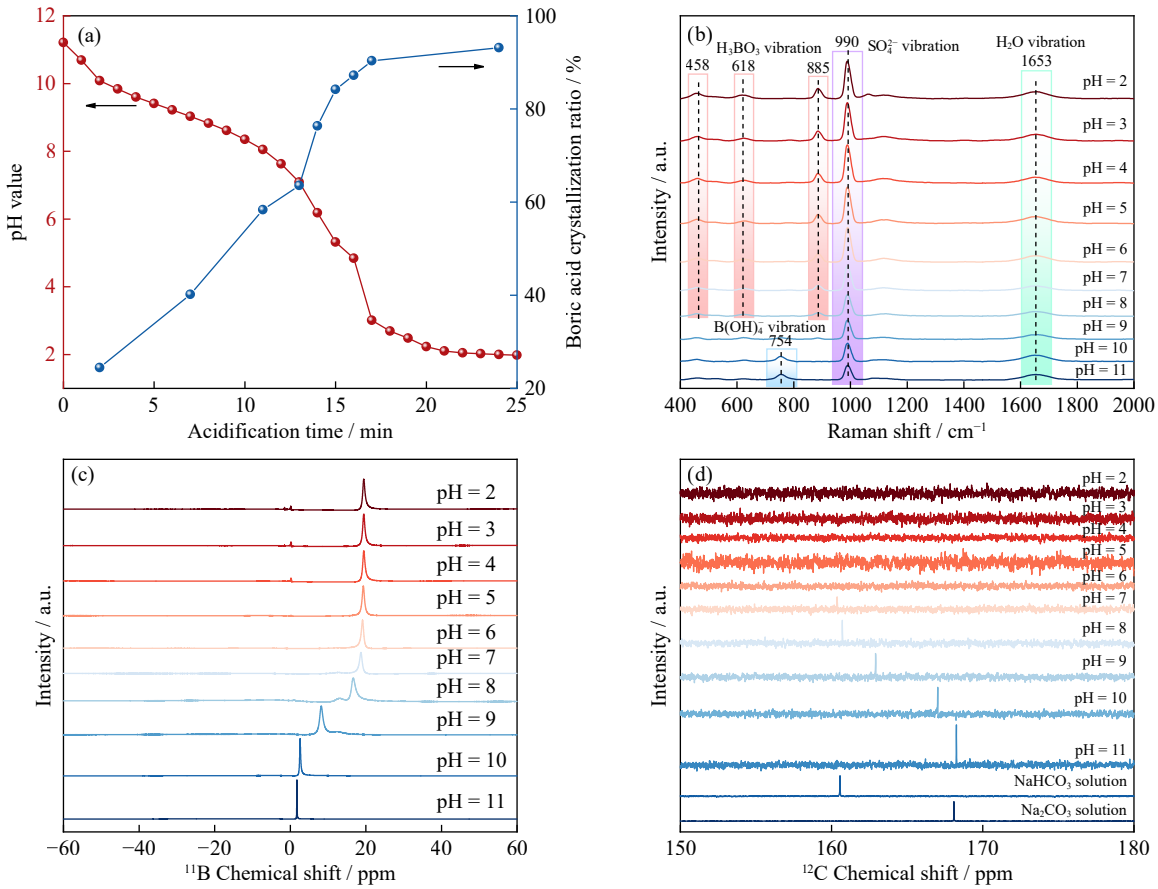

Fig. 9. (a) pH value of the solution varied with the acidification time; (b) Raman spectra, (c) ^{11}B and (d) ^{12}C NMR spectra of the solution with different pH values at 298 K.

at 990 cm^{-1}, corresponding to the symmetric stretching vibrations of free SO_4^{2-} ions, gradually enhanced, demonstrating that the SO_4^{2-} ions concentration increased with the decrease of pH value [22–23]. The Raman band at 1653 cm^{-1} is ascribed to the water H–O–H bending mode [24]. ^{11}B and ^{12}C NMR spectra analyses are further conducted to characterize the variation of boron and carbon species during the acidification process.

As shown in Fig. 9(c), the ^{11}B chemical shift significantly shifted to the positive direction with a decrease in the pH value, suggesting that the chemical coordination environment had altered. There is a sharp peak at ^{11}B chemical shift of about 1.7 ppm that was identified as peak of $B(OH)_4^-$ species, when the pH value of the solution was 11.0 or 10.0 [25–26]. When the pH value decreased to 9.0, the chemical shift was observed at 8.2 ppm, corresponding to the presence of polyborate anions [27]. As the pH value of the solution continued to decrease to 7.0 and below, the chemical shift of the resonance peak slightly changed and remained at about 19.5 ppm, which is ascribed to H_3BO_3 [28–29]. From the ^{12}C NMR spectra (Fig. 9(d)), the chemical shift evidently shifted to the low chemical shift direction with a decrease in the pH value, and the intensity of the resonance peak was noticeably weakened and disappeared at pH of 6.0. When the pH value of the solution decreased from 11.0 to 7.0, the ^{12}C chemical shift transformed from 168.1 to 160.3 ppm, demonstrating the carbon species converted from CO_3^{2-} ions to HCO_3^- ions [30–31]. These results demonstrate the effective synthesis of high-purity boric acid by adjusting the pH of the boron-rich liquor using sulfuric acid, as shown in Eqs. (10)–(13).

$$SiO_2(OH)_2^{2-}(aq) + 2H^+(aq) = SiO_2 \cdot H_2O(s) + H_2O(l) \quad (10)$$

$$B(OH)_4^-(aq) + H^+(aq) = H_3BO_3(aq) + H_2O(l) \quad (11)$$

$$CO_3^{2-}(aq) + H^+(aq) = HCO_3^-(aq) \quad (12)$$

$$HCO_3^-(aq) + H^+(aq) = CO_2(g) + H_2O(l) \quad (13)$$

3.2.3. Characterization of boric acid

When adjusting the pH of the solution to less than 7.0, the silicic acid precipitates from the solution. After filtering out the silica ($SiO_2 \cdot nH_2O$), the liquor was subjected to fractional crystallization to acquire boric acid and sodium sulfate, respectively. Chemical analysis results indicate that the purity of boric acid reached 99.5wt%. Fig. 10(a) shows that the XRD pattern of as-synthesized boric acid well matched with the standard PDF card (PDF#73-2158), and no impurity peak was observed, indicating that the synthesized boric acid with a high purity. Interestingly, compared with the XRD pattern of commercial boric acid agent, only a diffraction peak corresponding to the (002) crystal plane was observed in the as-synthesized boric acid, revealing that the preferential growth orientation of the (002) plane occurs. Raman spectroscopy was further used to characterize the structure of as-synthesized boric acid, as shown in Fig. 10(b). The band at 885 cm^{-1} is quite intense and attributed to the

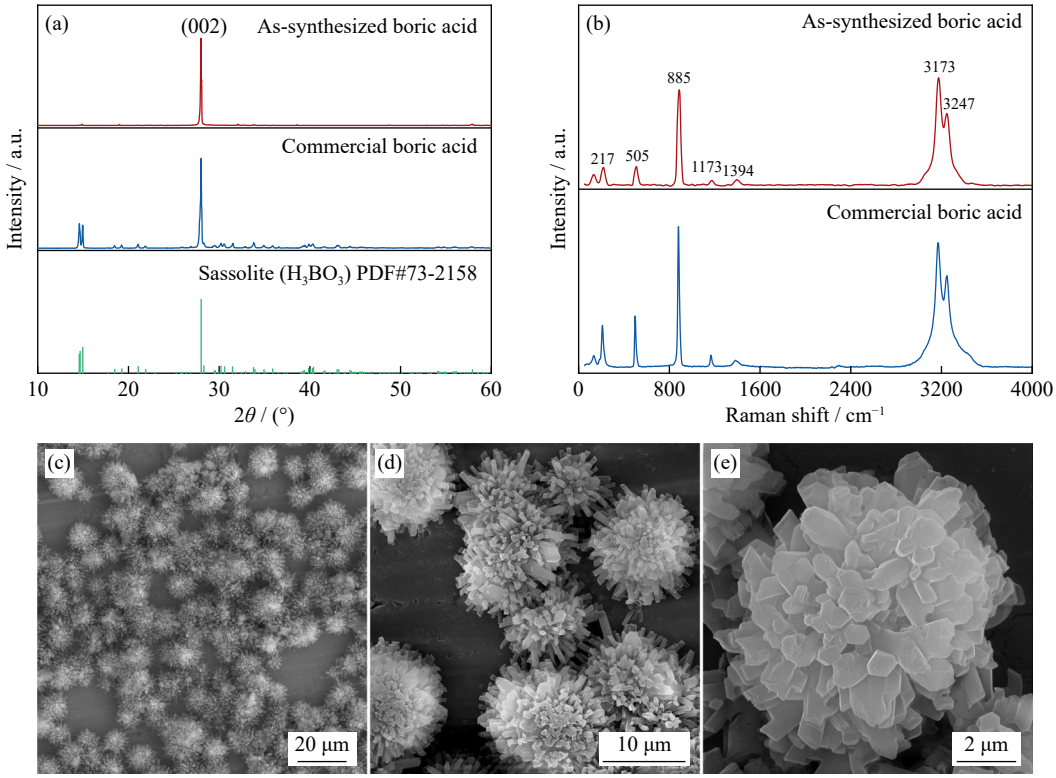

Fig. 10. (a) XRD patterns, (b) Raman spectrum, and (c–e) SEM images of as-synthesized boric acid.

symmetric stretching vibrations of B–O bonds, and the bands at 505, 1173, and 1394 cm^{-1} are assigned to H_3BO_3 [19,32–33]. The wide bands at 3173 and 3247 cm^{-1} are attributed to the H–O vibrations. SEM images (Fig. 10(c)–(e)) display that the synthesized boric acid presents petal-like microstructures with a particle size of about 10 μm. Additionally, the shape of the particles is rather regular, and the surface is smooth and clean, indicating that excellent crystallization and high purity.

Fig. 11(a) shows that all diffraction peaks in XRD pattern of crystallized sodium sulfate are well indexed to the standard PDF card (PDF#70-1541). SEM images (Fig. 11(b)–(c)) show that the sodium sulfate product was composed of rod-like particles with a size of 0.5–1 μm.

Based on the results obtained, an integrated process was established, and the chemical composition and elemental distribution of the various products are presented in Table 3.

3.3. Economic analysis and process evaluation

Fig. 12 presents a comparative analysis of the economic and technical indicators associated with the traditional process and the proposed process. Taking 1000 kg of ludwigite ore as a basis, the input costs of the raw materials (ludwigite ore, CO_2, and soda-ash) and energy consumption for the traditional process were $53.96 and $104, respectively. The revenue generated from the products (hot metal and borax) was $236.2, resulting in a net profit of $77.6 for the entire process. In contrast, for the novel process, the input costs for the raw materials (ludwigite ore, lignite, soda-ash, and sulfuric acid) and energy consumption were $87.2 and $107.4, respectively. The revenue from products (reduced iron powder, boric acid, and sodium sulfate) totaled $301, and the net profit of the integrated process was $106.4. More details of the economic calculation are provided in Table S4 and S5. Therefore, the novel process proposed in this study demonstrates superior economic feasibility for treating ludwigite ore at the current laboratory scale.

In the novel process, ludwigite ore is initially subjected to gradient magnetic separation to obtain BIMC. This mixed

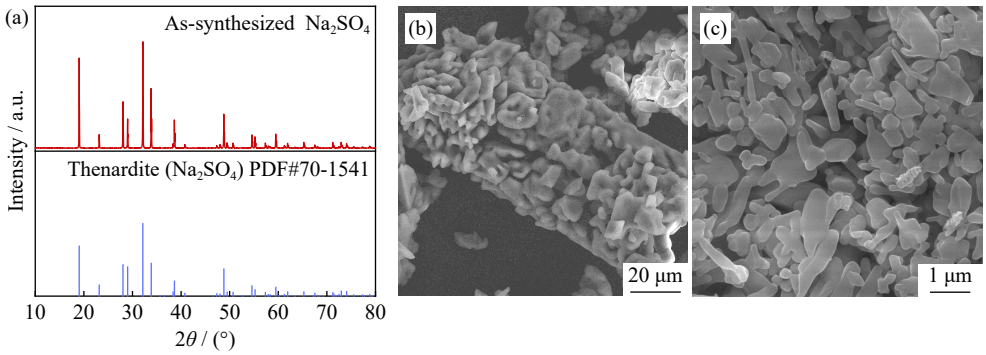

Fig. 11. (a) XRD patterns and (b–c) SEM images of synthesized sodium sulfate.

Table 3. Chemical composition and elemental distribution of various products

Sample	Mass / g	Chemical composition / wt%					Elemental distribution / %				
		B_2O_3	TFe	Na_2O	MgO	SiO_2	B_2O_3	TFe	Na_2O	MgO	SiO_2
Raw ore	100.00	5.80	46.89	0.01	15.31	7.64	—	—	—	—	—
Roasted ore	95.30	6.09	49.20	15.34	16.07	8.02	100.00	100.00	100.00	100.00	100.00
Magnetic concentrate	46.51	0.47	94.12	0.26	1.23	1.22	3.95	93.35	0.87	3.92	7.42
Tailing	39.72	3.77	7.85	12.06	37.03	16.48	25.82	6.65	33.42	96.08	85.67
Leached liquor	1.00[a]	4.07[b]	—	9.61[b]	—	0.53[b]	70.23	—	65.71	—	6.91
Boric acid	6.75	57.28	—	—	—	—	65.41	—	—	—	—
Sodium sulfate	21.80	—	—	43.64	—	—	—	—	65.05	—	—
Mother liquid	1.00[a]	0.27[b]	—	0.10[b]	—	0.53[b]	4.82	—	0.66	—	6.91

Note: a—the volume of product, L; b—the concentration of the component, g/L.

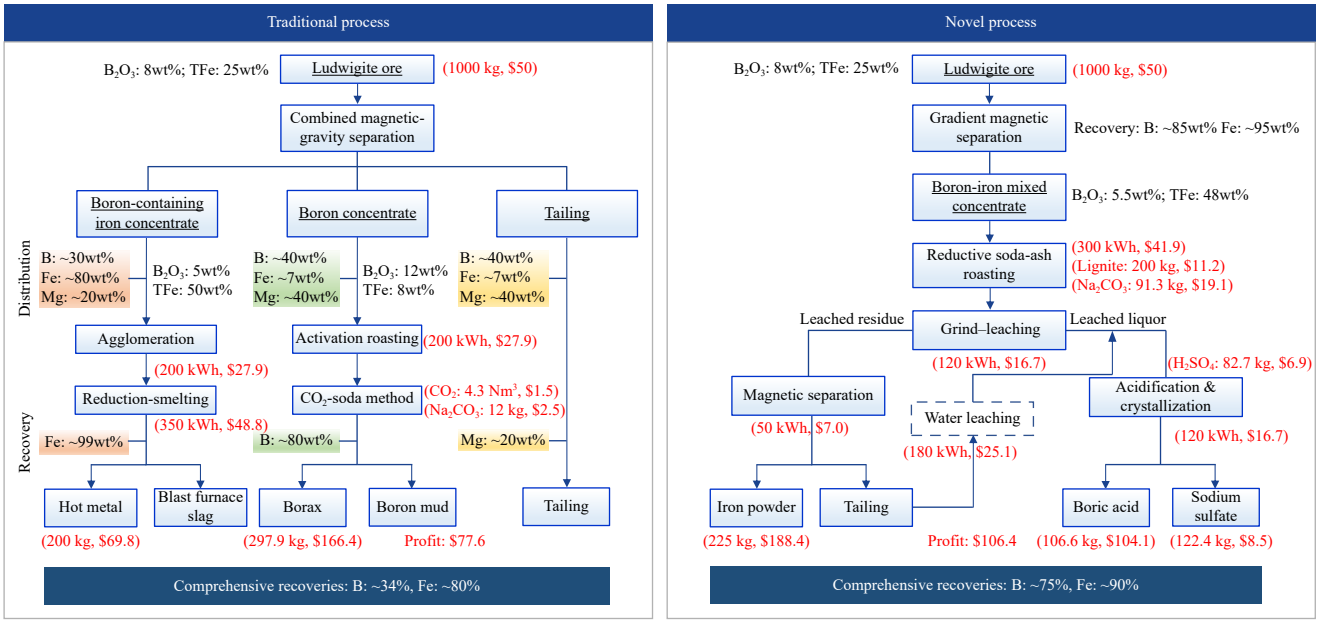

Fig. 12. Economic analysis of the traditional and novel process for boron and iron recovery from the ludwigite ore.

concentrate then undergoes reductive soda-ash roasting, which facilitates the simultaneous activation of boron and the reduction of iron oxides. Subsequently, through magnetic separation, acidification, and fractional crystallization, reduced iron powder and boric acid are produced. This method directly utilizes the BIMC as the raw material, thereby breaking the limitations of traditional ludwigite ore treatment that necessitate the pre-separation of boron and iron. This innovation significantly improves the recoveries of both boron and iron. Furthermore, the proposed process integrates the smelting of iron concentrate with the chemical processing of boron concentrate into a single operation. This integration simplifies the overall process, significantly improves the recoveries of boron and iron, reduces solid waste emissions, and notably eliminates the generation of boron mud.

4. Conclusions

This study successfully demonstrated an integrated process for producing reduced iron powder and boric acid from reductive soda-ash roasted BIMC in a rotary kiln. The key findings are summarized as follows:

(1) Rotary kiln reduction results indicated that the dosage of lignite significantly influenced the iron metallization ratio. Through a combination of wet-grinding and magnetic separation, under optimized conditions (roasting temperature of 1323 K, 8wt% lignite addition, duration of 60 min, grinding time of 20 min, pulp concentration of 50wt%, and a magnetic field intensity of 79.6 $kA \cdot m^{-1}$), a boron leaching efficiency of 70.23%, an iron grade in the magnetic concentrate of 94.12wt%, and an iron recovery of 93.35% were achieved. The synergistic effect of grinding and leaching not only refined mineral particles but also enhanced boron dissolution.

(2) The boric solution chemistry revealed that boron and silicon existed as boric acid (H_3BO_3) and silicic acid ($SiO_2 \cdot H_2O$), respectively, at pH values below 7.0. Raman and ^{11}B NMR spectroscopy confirmed the transformation of boron species from $B(OH)_4^-$ ions to polyborate ions ($B_3O_3(OH)_4^-$ or $B_4O_5(OH)_4^{2-}$ ions) and finally to H_3BO_3 as the pH decreased from 11.0 to 2.0. Similarly, ^{12}C NMR spectroscopy showed the conversion of carbon species from CO_3^{2-} to HCO_3^- and then to CO_2 gas.

(3) By adjusting the pH using sulfuric acid, silicic acid precipitated first and was removed by filtration. Fractional

crystallization, leveraging solubility differences, was employed to prepare boric acid and recover sodium sulfate. The as-prepared high-purity boric acid (99.5wt%) exhibited preferential growth orientation of the (002) crystal plane, with a petal-like morphology and a particle size of 10 μm.

Acknowledgements

This work was financially supported by the China National Postdoctoral Program for Innovative Talents (No. BX20250037), and the Key Lab of Critical Metals Minerals Supernormal Enrichment and Extraction, Ministry of Education (No. GJJSKFYB202505).

Conflict of Interest

The authors declare that they have no known competing financial interests or personal relationships that could have appeared to influence the work reported in this paper.

Supplementary Information

The online version contains supplementary material available at https://doi.org/10.1007/s12613-025-3238-z.

References

[1] J. An and X.X. Xue, Life cycle environmental impact assessment of borax and boric acid production in China, *J. Cleaner Prod.*, 66(2014), p. 121.

[2] X.J. Fu, J.Q. Zhao, S.Y. Chen, Z.G. Liu, T.L. Guo, and M.S. Chu, Comprehensive utilization of ludwigite ore based on metallizing reduction and magnetic separation, *J. Iron Steel Res. Int.*, 22(2015), No. 80, p. 672.

[3] X.J. Fu, M.S. Chu, L.H. Gao, and Z.G. Liu, Stepwise recovery of magnesium from low-grade ludwigite ore based on innovative and clean technological route, *Trans. Nonferrous Met. Soc. China*, 28(2018), No. 11, p. 2383.

[4] L. Ye, Z.W. Peng, R. Tian, *et al*., A novel process for highly efficient separation of boron and iron from ludwigite ore based on low-temperature microwave roasting, *Powder Technol.*, 410(2022), art. No. 117848.

[5] M.S. Chu, J.Q. Zhao, X.J. Fu, and Z.G. Liu, New efficient process utilizing ludwigite on gas-based shaft furnace direct reduction and electric furnace smelting separation, *J. Northeast. Univ.* (*Nat. Sci.*), 37(2016), No. 6, p. 805.

[6] G.J. Cheng, X.Z. Liu, H. Yang, X.X. Xue, and L.J. Li, Sintering and smelting property investigations of ludwigite, *Processes*, 10(2022), No. 1, art. No. 159.

[7] G. Wang, J.S. Wang, Y.G. Ding, S. Ma, and Q.G. Xue, New separation method of boron and iron from ludwigite based on carbon bearing pellet reduction and melting technology, *ISIJ Int.*, 52(2012), No. 1, p. 45.

[8] Q.P. Bao, L. Guo, H.Y. Sohn, *et al*., New process for treating boron-bearing iron ore by flash reduction coupled with magnetic separation, *Int. J. Miner. Metall. Mater*, 31(2024), No. 3, p. 473.

[9] J.X. You, J. Wang, J. Luo, Z.W. Peng, M.J. Rao, and G.H. Li, A facile route to the value-added utilization of ludwigite ore: Boron extraction and $M_xMg_{1-x}Fe_2O_4$ spinel ferrites preparation, *J. Cleaner Prod*, 375(2022), atr. No. 134206.

[10] J.X. You, J. Wang, M.J. Rao, *et al*., An integrated and efficient process for borax preparation and magnetite recovery from soda-ash roasted ludwigite ore under $CO–CO_2–N_2$ atmosphere, *Int. J. Miner. Metall. Mater.*, 30(2023), No. 11, p. 2169.

[11] G.H. Li, B.J. Liang, M.J. Rao, Y.B. Zhang, and T. Jiang, An innovative process for extracting boron and simultaneous recovering metallic iron from ludwigite ore, *Miner. Eng.*, 56(2014), p. 57.

[12] B.J. Liang, G.H. Li, M.J. Rao, Z.W. Peng, Y.B. Zhang, and T. Jiang, Water leaching of boron from soda-ash-activated ludwigite ore, *Hydrometallurgy*, 167(2017), p. 101.

[13] Z.P. Zhu, J.X. You, X. Zhang, *et al*., Recycling excessive alkali from reductive soda ash roasted ludwigite ore: Toward a zero-waste approach, *ACS Sustainable Chem. Eng.*, 8(2020), No. 13, p. 5317.

[14] S. Bhagyaraj, M.A. Al-Ghouti, P. Kasak, and I. Krupa, An updated review on boron removal from water through adsorption processes, *Emergent Mater.*, 4(2021), No. 5, p. 1167.

[15] M. Dolati, A.A. Aghapour, H. Khorsandi, and S. Karimzade, Boron removal from aqueous solutions by electrocoagulation at low concentrations, *J. Environ. Chem. Eng.*, 5(2017), No. 5, p. 5150-5156.

[16] F.L. Theiss, G.A. Ayoko, and R.L. Frost, Removal of boron species by layered double hydroxides: A review, *J. Colloid Interface Sci.*, 402(2013), p. 114.

[17] Y.Q. Zhou, C.H. Fang, Y. Fang, and F.Y. Zhu, Polyborates in aqueous borate solution: A Raman and DFT theory investigation, *Spectrochim. Acta Part A*, 83(2011), No. 11, p. 82.

[18] F.Y. Zhu, W.Q. Zhang, H.Y. Liu, Y.Q. Zhou, X.F. Wang, and C.H. Fang, Raman and ab initio analyses of ion pairs in concentrated $K[B(OH)_4]$ droplets, *Spectrochim. Acta Part A*, 230(2020), art. No. 118039.

[19] F. Spadaro, A. Rossi, S.N. Ramakrishna, E. Lainé, P. Woodward, and N.D. Spencer, Understanding complex tribofilms by means of $H_3BO_3–B_2O_3$ model glasses, *Langmuir*, 34(2018), No. 6, p. 2219.

[20] H.H. Liu, Q. Liu, Y.S. Lan, *et al*., Speciation of borate in aqueous solutions studied experimentally by potentiometry and Raman spectroscopy and computationally by DFT calculations, *New J. Chem.*, 47(2023), No. 18, p. 8499.

[21] L.M.S.G.A. Applegarth, C.C. Pye, J.S. Cox, and P.R. Tremaine, Raman spectroscopic and ab initio investigation of aqueous boric acid, borate, and polyborate speciation from 25 to 80°C, *Ind. Eng. Chem. Res.*, 56(2017), No. 47, p. 13983.

[22] P.V. Jentzsch, B. Kampe, P. Rösch, and J. Popp, Raman Spectroscopic study of crystallization from solutions containing $MgSO_4$ and Na_2SO_4: Raman spectra of double salts, *J. Phys. Chem. A*, 115(2011), No. 22, p. 5540.

[23] H. Cui, R.C. Zhong, Z.M. Li, *et al*., The temperature dependence of Raman intensity of aqueous species (SO_4^{2-} and $H_3PO_4^0$): Implication for *in situ* fluid composition investigation at elevated temperature, *Chem. Geol.*, 617(2013), art. No. 121261.

[24] R.L. Frost, J. Čejka, J. Sejkora, D. Ozdín, S. Bahfenne, and E.C. Keeffe, Raman spectroscopic study of the antimonate mineral brandholzite $Mg[Sb_2(OH)_{12}]·6H_2O$, *J. Raman Spectrosc.*, 40(2009), No. 12, p. 1907.

[25] W. Chen, L.Z. Ouyang, J.W. Liu, *et al*., Hydrolysis and regeneration of sodium borohydride (NaBH4)−A combination of hydrogen production and storage, *J. Power Sources*, 359(2017), p. 400.

[26] L.Z. Ouyang, W. Chen, J.W. Liu, M. Felderhoff, H. Wang, and M. Zhu, Enhancing the regeneration process of consumed $NaBH_4$ for hydrogen storage, *Adv. Energy Mater.*, 7(2017), No. 19, art. No. 1700299.

[27] M.J. Verma and P.A. Deshpande, Computational insights into

biomimetic CO_2 hydration activities of (poly)borate ions, *J. Phys. Chem. C*, 121(2017), No. 32, p. 17197.

[28] A. Filippov, O.N. Antzutkin, and F.U. Shah, Understanding the interaction of boric acid and CO_2 with ionic liquids in aqueous medium by multinuclear NMR spectroscopy, *ACS Sustainable Chem. Eng.*, 8(2020), No. 1, p. 552.

[29] Y.Z. Chen, J.F. Lyu, Y.M. Wang, *et al*., Synthesis, characterization, adsorption, and isotopic separation studies of pyrocatechol-modified MCM-41 for efficient boron removal, *Ind. Eng. Chem. Res.*, 58(2019), No. 8, p. 3282.

[30] O.F. Yasar, W.C. Liao, B. Stevensson, and M. Edén, Structural role and spatial distribution of carbonate ions in amorphous calcium phosphate, *J. Phys. Chem. C*, 125(2021), No. 8, p. 4675.

[31] X.E. Hu, Q. Yu, F. Barzagli, *et al*., NMR techniques and prediction models for the analysis of species formed in CO_2 capture processes with amine-based sorbents: A critical review, *ACS Sustainable Chem. Eng.*, 8(2020), No. 16, p. 6173.

[32] L.A.L. Dias and W.A. Alves, Spectroscopic and conductometric behavior of boric acid in water and in an aprotic polar solvent, *J. Mol. Liq.*, 289(2019), art. No. 111152.

[33] H. Arcis, J.P. Ferguson, L.M.S.G.A. Applegarth, G.H. Zimmerman, and P.R. Tremaine, Ionization of boric acid in water from 298 K to 623 K by AC conductivity and Raman spectroscopy, *J. Chem. Thermodyn.*, 106(2017), p. 187.